JGR Oceans

RESEARCH ARTICLE
10.1029/2019JC015064

Direct Measurements of Upper Ocean Horizontal Velocity and Vertical Shear in the Tropical North Atlantic at 4°N, 23°W

Renellys C. Perez[1], Gregory R. Foltz[1], Rick Lumpkin[1], and Claudia Schmid[1]

[1]NOAA/AOML, Miami, FL, USA

Key Points:
- Observations in the tropical North Atlantic yield new insights into the structure of upper ocean velocity and vertical shear
- Mean zonal velocity and vertical shear were strongest below 30 m, and near-surface mean eastward currents were weaker than long-term mean
- Tropical instability waves were observed with energetic meridional velocity fluctuations and modest vertical shear compared to winter/spring

Correspondence to:
R. C. Perez,
renellys.c.perez@noaa.gov

Citation:
Perez, R. C., Foltz, G. R., Lumpkin, R., & Schmid, C. (2019). Direct measurements of upper ocean horizontal velocity and vertical shear in the tropical North Atlantic at 4°N, 23°W. *Journal of Geophysical Research: Oceans*, *124*. https://doi.org/10.1029/2019JC015064

Received 19 FEB 2019
Accepted 25 APR 2019
Accepted article online 6 MAY 2019

Abstract The Tropical Atlantic Current Observations Study measured upper ocean horizontal velocity from a mooring at 4°N, 23°W, at discrete depths between 7 and 87 m, in order to observe the temporal and vertical structure of the currents. Between March 2017 and March 2018, mean zonal velocity and vertical shear were strongest between 32 and 37 m. Near-surface mean eastward currents during this period were weaker than the long-term mean but within the range of previously observed values given the high interannual variability. Interannual variability of the zonal velocity exceeded that of the meridional velocity, was primarily geostrophically driven, and was strongly influenced by the large-scale currents. Energetic tropical instability waves (TIWs) were observed in early summer and late fall of 2017. Meridional velocity fluctuations associated with the TIWs were far larger than those of zonal velocity and extended down to 87 m. These fluctuations propagated upward to the surface with vertical phase speeds between 12 and 15 m/day. Coherent velocity and vertical shear variations emerged in a TIW composite. However, the vertical shears observed during the TIW season were modest compared to the large shear measured in spring 2017 and winter 2018. As a result, TIWs may be less crucial for vertical turbulent cooling at 4°N, 23°W than they are near the equator. To observe the intense winter/spring vertical shear events, fine vertical (less than 10 m) and diurnal temporal sampling is needed.

Plain Language Summary Changes in upper ocean currents influence temperature, salinity, and air-sea fluxes in the tropical North Atlantic, which in turn affect the weather, climate, and fisheries of the surrounding continents. The Tropical Atlantic Current Observations Study measured upper ocean currents and vertical shear of velocity for the first time at a moored buoy at 4°N, 23°W. These data yielded several new insights: The average zonal currents and vertical shear are strongest at a depth of 32 to 37 m below the surface. Both the average east-west and north-south currents are fairly weak relative to strong high-frequency fluctuations in the north-south currents associated with tropical instability waves (TIWs). However, vertical shears observed during the TIW season were modest compared to large shear measured in spring 2017 and winter 2018. This suggests that TIWs at 4°N, 23°W may be less crucial for vertical turbulent cooling and upper ocean temperature budgets than they are near the equator. Given the high year-to-year variability in zonal velocity at this location, partly driven by changes in the large-scale background currents, multiple years of fine vertical scale (less than 10-m spacing) and high-frequency (subdiurnal) velocity and shear data are needed to evaluate the robustness of these findings.

1. Introduction

The tropical Atlantic plays an important role in shaping the basin-wide upper-ocean circulation and coupled ocean-atmosphere variability. This is especially true in the latitude range of the intertropical convergence zone (2–12°N). Here sea surface temperature (SST) is strongly coupled to the surface wind, and large SST anomalies can lead to extreme drought or floods in Northeast Brazil (Foltz et al., 2012; Nobre & Shukla, 1996; Rugg et al., 2016) and affect Atlantic hurricane activity (Goldenberg & Shapiro, 1996; Kossin & Vimont, 2007). The southern intertropical convergence zone region also experiences strong intraseasonal and seasonal SST and velocity fluctuations from tropical instability waves (TIWs; e.g., Grodsky et al., 2005; Perez et al., 2012, 2014; von Schuckmann et al., 2008) and shallow meridional tropical circulation cells (e.g., Helber et al., 2007; Molinari et al., 2003; Perez et al., 2014). The tropical circulation cells provide an important pathway for seasonal and interannual heat exchange between the equatorial Atlantic cold tongue and surrounding regions, yet there are few direct observations of their temporal evolution and vertical structure and how they are influenced by subseasonal wind-driven events and TIWs (Burmeister et al., 2016;

Published 2019. This article is a U.S. Government work and is in the public domain in the USA.

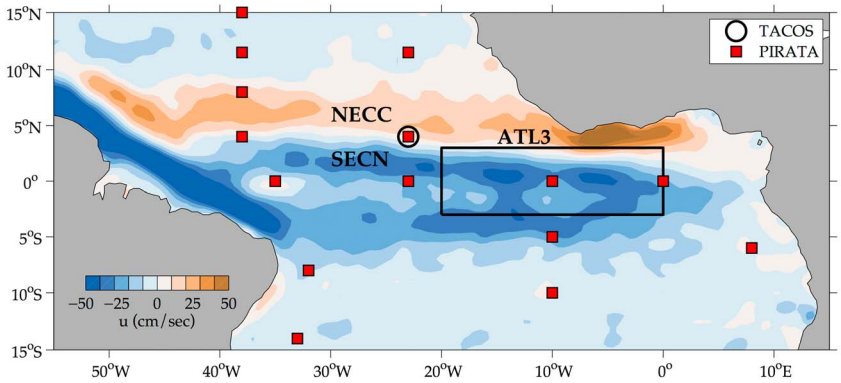

Figure 1. Mean near-surface zonal velocity in the tropical Atlantic from the Lumpkin and Johnson (2013) drifter climatology. Brown color shading indicates eastward currents, and blue color shading indicates westward currents. The symbols show the locations of the Prediction and Research Moored Array in the Tropical Atlantic (PIRATA) moorings located between 15°S and 15°N (red squares) and the Tropical Atlantic Current Observations Study (TACOS) deployment (black circle). The black box identifies the region over which the ATL3 sea surface temperature index is computed. The northern branch of the westward flowing South Equatorial Current (SECN) and the eastward flowing North Equatorial Countercurrent (NECC) are identified.

Lubbecke, 2013; Perez et al., 2014; Peter et al., 2006; Richter et al., 2013). TIWs modulate horizontal and vertical ocean heat fluxes and turbulent mixing, both of which strongly influence near-equatorial SST (e.g., Foltz et al., 2003; Hummels et al., 2013). However, far less is known about the impacts of TIWs and shorter-duration variations such as internal waves and near-inertial waves north of the equator, due to a lack of continuous horizontal velocity and vertical shear data in the upper 100 m of the water column. Most off-equatorial observations of shear and mixing come from limited microstructure profiles (Hummels et al., 2013, 2014). This study examines how velocity and shear vary over the course of a year using a new velocity data set from a mooring in the tropical North Atlantic.

Although there has been a long history of observing velocity variations in the tropical Atlantic with moored buoys (e.g., Brandt et al., 2008; Brandt et al., 2014; Grodsky et al., 2005; Johns et al., 2014; Perez et al., 2014; Weisberg et al., 1987; Wenegrat & McPhaden, 2015), there is a paucity of velocity data poleward of ±2° latitude. Previous studies of off-equatorial velocity in the tropical Atlantic have relied on time series measurements from a limited number of point current meters (Perez et al., 2012, 2014; Weisberg & Weingartner, 1988) or moored Acoustic Doppler Current Profilers (ADCPs) which do not observe the upper 30 m (e.g., Brandt et al., 2008; Perez et al., 2014). Other sampling platforms can resolve elements of the off-equatorial flow but are limited in terms of their temporal or spatial coverage. These include gridded surface velocity products from drifters and Argo floats, satellite altimetry and/or drifter-altimetry syntheses (e.g., Brandt et al., 2006; Helber et al., 2007; Hormann et al., 2012, 2013; Lumpkin & Garzoli, 2005; Schmid et al., 2001), and two-dimensional cross-sections of velocity from repeated hydrographic and ADCP sections (e.g., Brandt et al., 2006; Goes et al., 2013; Perez et al., 2014).

The Tropical Atlantic Current Observations Study (TACOS) was designed to measure upper ocean velocity and vertical shear at the 4°N, 23°W Prediction and Research Moored Array in the Tropical Atlantic (PIRATA) mooring (Figure 1; Bourlès et al., 2008; 2019). For the first time, the TACOS data provide a high-resolution 1-year (March 2017 to March 2018) view of the temporal and vertical structure of the currents at this location. The mooring sits north of the mean boundary between the northern branch of the westward flowing South Equatorial Current (SECN) and the eastward flowing North Equatorial Countercurrent (NECC; Garzoli & Katz, 1984; Brandt et al., 2006; Brandt et al., 2010; Hormann et al., 2012), where northward wind-driven currents are expected at the surface and the southward geostrophic flow of the tropical circulation cells is present underneath (e.g., Perez et al., 2014). Here we present results from the first year of TACOS observations. We focus on the mean vertical structure of horizontal velocity and vertical current shear, strong intraseasonal fluctuations from TIWs, and their impact on velocity, vertical shear, and temperature. Ancillary data and output from ocean reanalysis products and a numerical simulation are used to provide longer-term context on the background state of the tropical Atlantic circulation and the factors that control year-to-year variability in the vicinity of the mooring. We will also briefly

Table 1
Mean and standard deviation (σ) of zonal velocity (u), meridional velocity (v), and velocity magnitude (U) at 4°N, 23°W for each sensor depth (z)

z (m)	Record length (days)	Mean (σ) u (cm/s)	Mean (σ) v (cm/s)	Mean (σ) U (cm/s)
7	300.25	2.81 (18.04)	5.52 (27.95)	29.16 (17.16)
12	380.83	2.41 (17.77)	4.34 (25.48)	27.14 (15.90)
17	383.67	3.27 (17.35)	2.63 (24.36)	25.92 (15.51)
22	383.71	5.27 (16.98)	1.53 (23.64)	25.35 (15.31)
27	383.88	6.40 (16.52)	-0.13 (23.43)	25.14 (15.20)
32	383.96	8.03 (16.18)	-0.78 (23.37)	25.28 (15.28)
37	109.80	9.86 (14.60)	-8.73 (21.75)	25.42 (14.60)
37 (gaps filled)	383.96	8.58 (15.31)	-1.93 (22.58)	24.38 (15.08)
47	373.63	8.39 (15.90)	-3.29 (22.97)	24.74 (15.79)
57	381.08	7.22 (16.23)	-3.63 (22.43)	24.16 (15.75)
66.6	381.79	6.27 (16.05)	-3.17 (20.99)	22.97 (14.83)
86.6	127.42	-3.25 (10.51)	-2.56 (12.12)	13.56 (9.52)

Note. Instruments were deployed on 6 March 2017 and recovered on 26 March 2018. Means and standard deviations after gaps have been filled (see section 2) are also provided for the 37-m sensor.

discuss the wider implications of the TACOS results for observing horizontal velocity and vertical shear in the tropical North Atlantic.

2. Data and Models

2.1. Hourly Mooring Data

In March 2017, a T-Flex mooring developed by NOAA/PMEL was deployed at the 4°N, 23°W PIRATA site (Bourlès et al., 2019). As is typical for these moorings, it has a suite of meteorological sensors and a combination of temperature, conductivity, and pressure sensors in the upper 500 m, as well as a single point acoustic current meter at 12-m depth (Bourlès et al., 2019). The PIRATA mooring at this site prior to March 2017 measured currents at 10-m depth (Bourlès et al., 2008; Perez et al., 2014). We augmented the velocity measurements at this mooring with 10 additional point acoustic current meters distributed between the surface and 90-m depth, with a vertical spacing ranging from 5 to 20 m. These current meters are downward facing and positioned so that their sample volumes are centered at 7, 12, 17, 22, 27, 32, 37, 47, 57, 66.6, and 86.6 m (hereafter, the last two will be referred to as 67 and 87 m, respectively).

TACOS instruments collected up to 384 days of hourly real-time velocity data. Duration and record-length statistics (mean and standard deviation) are documented in Table 1. Data return rates for the instruments exceeded 99% at all depths, except at 7, 37, and 87 m where the instruments stopped early and return rates are 78.2%, 28.6%, and 33.2%, respectively. These instruments failed due to prematurely depleted batteries that resulted in extreme voltage drops shortly before the end of the record. The voltage drops did not adversely affect the velocity data prior to the batteries being depleted, except likely at 7 m starting in mid-October 2017, when some spurious high-frequency (subdaily) velocity and shear differences between 7 and 12 m were detected. These high-frequency differences did not significantly affect the filtered (48-hr low-pass) velocity, as the filtered 7- and 12-m velocities agreed well with one another throughout the whole time period of overlap ($r > 0.95$, compare red and black lines in Figures 2a and 2b) compared to the agreement prior to October 15 ($r > 0.98$). However, these differences did cause subdaily variations in 7- to 12-m vertical shear that were not observed in other depth ranges (e.g., 12- to 17-m and 17- to 22-m shear). Therefore, for the vertical shear analysis presented in this paper, we only consider 7- to 12-m shear prior to October 15.

During post cruise calibration spin tests of the TACOS instruments, compass calibration offsets were detected for the eight sensors which still had a functioning battery (e.g., all sensors except 7, 37, and 87 m). This compass offset did not affect the magnitude of the flow but may have introduced an instantaneous error in the orientation of the flow at each sensor. This error varies with compass orientation and is typically largest when flow is southwestward. The mean compass bias is less than ±5° with a standard error of less than 2° for all sensors tested. Averaged over the full TACOS record and across all sensors tested, the magnitude of the resulting bias, $|b_c|$, was 0.9 cm/s for zonal velocity and 1.5 cm/s for meridional velocity. Similarly, the standard errors of the velocity error (e_c) averaged across all of the tested sensors were 0.3 cm/s for both zonal and meridional velocity. Because of the small uncertainty these compass errors may introduce into our TACOS-record means, we have conservatively expanded the TACOS velocity standard error bars (e_v) to be $(e_v^2 + e_c^2)^{1/2} + |b_c|$. These combined errors are shown as red error bars in Figures 2c and 2d.

At all depths, short (up to 6 hr) temporal gaps were filled with temporal interpolation. We decided not to vertically extrapolate and fill in the missing velocity data at 7 and 87 m after those sensors failed (Table 1). However, longer periods with missing velocity data at 37 m were filled via vertical interpolation using the hourly 32- and 47-m data (Table 1, red dashed lines in Figures 2c and 2d).

Concurrent hourly temperature data measured by the 4°N, 23°W PIRATA mooring at 1, 10, 20, 40, 60, 80, 100, 120, 180, 300, and 500 m were also used to examine upper ocean temperature variations. The depth of the thermocline, indicated by the 20 °C isotherm depth (Z20), is computed from the temperature data.

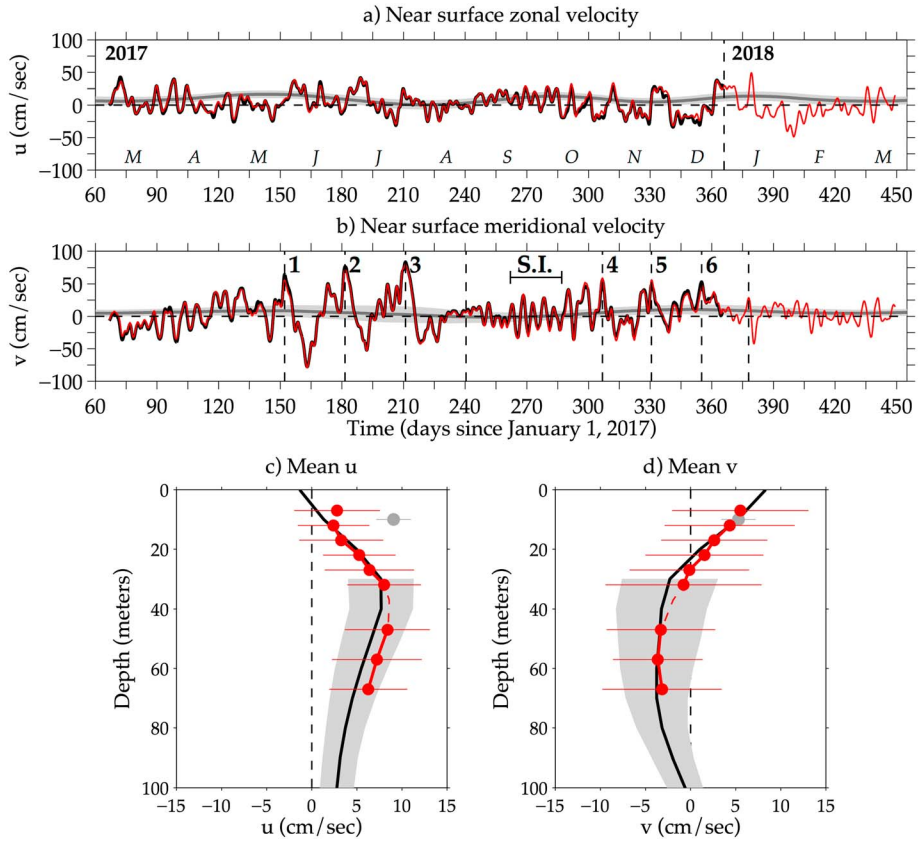

Figure 2. The 48-hr low-pass filtered time series of hourly (a) zonal and (b) meridional velocity at 7-m (black line) and 12-m depth (red line) at 4°N, 23°W during the Tropical Atlantic Current Observations Study (TACOS) deployment. The climatological seasonal cycle and associated standard errors of daily 10-m PIRATA velocities are shown as gray lines and shading, respectively. Numbers and characters in panel (a) correspond to years and months, and vertical lines with numbers in panel (b) correspond to the start/end times of 6 tropical instability waves. A period of superinertial (S.I.) oscillations is marked with a horizontal bar. TACOS mean (c) zonal and (d) meridional velocity as a function of depth (red dots with error bars). Red dashed lines indicate the impact of filling gaps at 37-m depth. Black lines show mean velocity profiles from Perez et al. (2014) acoustic Doppler current profiler sections combined with drifter data (ADCP+D), and gray shading shows the corresponding standard errors. Gray dots with error bars show the 10-m long-term mooring mean velocities and standard errors.

The moored velocity and temperature data exhibit significant variability at periods less than 2 days. This variability is primarily due to the diurnal cycle, tides, internal waves, and turbulent mixing and will be explored in detail in a later study. We focus on the 2-day and longer time scale events captured by the TACOS measurements. For the figures shown in this study, we have applied a 48-hr low-pass Bartlett (triangle) filter to the hourly data unless otherwise noted.

2.2. Ancillary Data and Models

Several additional in situ and satellite data products are used in this analysis. Daily gridded combined microwave SST produced by Remote Sensing Systems is available on a 0.25° grid from January 1998 to the present and is used to confirm the presence of TIWs in the TACOS mooring record (Figure 3). Near-surface (15-m) currents produced by NOAA's Global Drifter Program from a synthesis of drifter velocities, altimetry, and wind products (hereafter drifter-altimetry synthesis) are available as daily averages on a 0.25° grid from January 2013 to December 2017 (updated from Lumpkin & Garzoli, 2011 and Perez et al., 2012). These velocities are calculated poleward of 2.5°N by finding coefficients that minimize the mean square difference between drifter velocities and the sum of (a) a time mean velocity from Laurindo et al. (2017), (b) a gain coefficient times the concurrent geostrophic current anomalies computed from AVISO sea level, and (c) a downwind and cross-wind coefficient times the concurrent wind stress anomaly (representing the downwind and

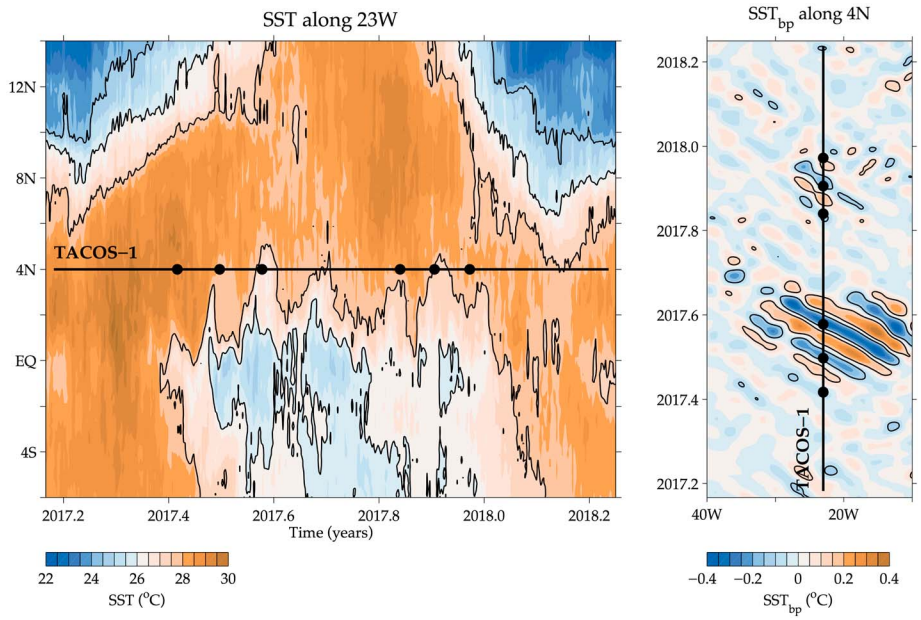

Figure 3. Temporal evolution of satellite sea surface temperature (SST) as a function of latitude along 23°W (left panel) and temporally and zonally band-pass filtered SST anomalies along 4°N (right panel) during the time period of the Tropical Atlantic Current Observations Study (TACOS) experiment. Black circles correspond to the maximum northward flow associated with the six tropical instability waves identified in Figure 2b.

cross-wind Ekman component of the current, including on the equator; Lumpkin & Garzoli, 2011; Niiler et al., 2003). These velocities are used to compare the background flow associated with the SECN and NECC during 2017 with annual means from 1993 to 2017 and to examine the Ekman and geostrophic contributions to those year-to-year variations. Daily near-surface (10-m) currents from the enhanced PIRATA (ePIRATA) data set, which combines daily PIRATA 10-m and 12-m velocity data from 2006 to 2017 and fills gaps with bias-corrected velocities from the aforementioned drifter-altimetry synthesis (Foltz et al., 2018), are also examined at 4°N, 23°W, to provide longer-term context for the TACOS measurements. Although ePIRATA daily temperature fields are also available from 2006 to 2017, here we only analyze hourly temperature data from the mooring during the TACOS experiment, to have collocated temperature and velocity measurements during the TACOS record.

Output from two global ocean reanalysis products with data assimilation, the ocean reanalysis system 4 (ORAS4; Balmaseda et al., 2013) from the European Centre for Medium-Range Weather Forecasts and the global ocean data assimilation system (GODAS; Behringer & Xue, 2004) from the National Centers for Environmental Prediction, are used to examine year-to-year variability of velocity in the upper 100 m. We also examine output from the global Ocean general circulation model for the Earth Simulator (OFES; Masumoto et al., 2004; Sasaki et al., 2008), which is forced with daily mean NCEP-NCAR reanalysis atmospheric data but does not assimilate observations. These models range from high (OFES: 0.1°) to intermediate (GODAS: 1° longitude × 1/3° latitude) to coarser (ORAS4: 1°) horizontal resolution. ORAS4 is available as monthly averages from 1980 to 2017. GODAS is available at higher temporal resolution (5-day averages from January 1980 to July 2018) as are OFES fields (3-day snapshots from 1980 to 2015). In the absence of suitable historical observations of subsurface velocity, the analysis of these models allows us to examine the representativeness of the vertical structure of an annual mean relative to a longer-term mean.

Over the whole PIRATA period and across all moorings, ORAS4 was found to compare better with 10-m ePIRATA velocities than GODAS in a study by Foltz et al. (2018). This is partly due to the fact that ORAS4 assimilates both PIRATA temperature and salinity, whereas GODAS only assimilates temperature from the moorings and assimilates synthetic salinity profiles. We include GODAS in our analysis because it provides 5-day averages during the entire first year of TACOS, whereas ORAS4 is only available as monthly fields. We include OFES because it is an eddy-resolving model that is available as 3-day snapshots. This

model has compared favorably against observations in the subtropical North and South Atlantic (e.g., Garzoli et al., 2015; Kersalé et al., 2019; Meinen et al., 2017; Perez et al., 2011; van Sebille et al., 2011, 2012; Zhao & Johns, 2014), and to our knowledge it has not yet been extensively used to study the tropical Atlantic.

3. Results

3.1. Near-Surface Velocities

TACOS velocities at 7- and 12-m depths are compared to the means and seasonal cycles obtained from the 4°N, 23°W PIRATA current meter at 10-m depth during 2006-2017 (Figures 2a and 2b). The seasonal cycles were created by grouping the 12-year record of the velocity data into daily bins according to calendar day and then averaging (gray line in Figures 2a and 2b). The uncertainties were estimated as the standard errors (gray shading in Figures 2a and 2b) associated with the daily means, assuming the daily observations in each year are independent of those in other years. A 90-day Bartlett low-pass filter was applied to these daily mean climatology and their standard error curves in Figures 2a and 2b to focus on the quarterly to annual variations in the historical record. To minimize the impact of temporal gaps in the long-term record of the 10-m velocity data (gray dots with lines for standard errors in Figures 2c and 2d), we remove the unfiltered daily seasonal cycle prior to computing the means.

The 12-year mean and standard errors of the flow at 10-m depth are 9.1 $\pm$ 1.9 cm/s eastward and 5.3 $\pm$ 1.9 cm/s northward (gray dots with lines in Figures 2c and 2d). The mean of the TACOS meridional velocity at 7 and 12 m agree well (i.e., they are not significantly different given the TACOS error bars, red dots with lines in Figure 2d) with the long-term mean PIRATA meridional velocity at 10 m. However, the mean near-surface TACOS zonal velocities are significantly weaker (2.8 $\pm$ 4.8 cm/s at 7 m and 2.4 $\pm$ 4.0 cm/s at 12 m) than the long-term moored estimate (red dots with lines in Figure 2c). The early termination of the 7-m record does not explain the discrepancy between the TACOS period and long-term mean zonal velocities, as the mean eastward velocity at 12 m was also weaker than the long-term PIRATA mean. This discrepancy will be examined in the context of year-to-year variations of the large-scale background currents using ancillary observations, models, and reanalysis products in section 4.

The 10-m zonal and meridional velocity seasonal cycles are weak with peaks and troughs that are not significantly distinguishable given the standard errors (gray lines with shading in Figures 2a and 2b). The mean climatological zonal velocity varies between 0 and 16 cm/s and is strongest in late boreal spring (gray line in Figure 2a, days 130-150), consistent with the mooring being near the mean position of the southern edge of the eastward flowing NECC, with fairly uniform standard errors (6 to 7 cm/s) throughout the year (gray shading). The 10-m mean meridional velocity climatology has a weak semiannual cycle, with 8-10 cm/s northward velocity in early summer (days 150–160) and early winter (days 325–350), and 2 cm/s southward flow during early fall (days 260–270, gray line in Figure 2b). The meridional velocity standard errors are largest (>9 cm/s) in summer and early fall (days 140–250), when the equatorial Atlantic cold tongue is strong and TIWs are typically active (e.g., Brandt et al., 2011; Caltabiano et al., 2005; Hormann et al., 2013; Perez et al., 2012; Wu & Bowman, 2007).

The range of the 7- and 12-m zonal velocities from TACOS (black and red lines in Figure 2a, respectively) is close to the long-term climatological velocity at 10 m (gray line). Although as mentioned earlier, the flow during TACOS is less strongly eastward than the climatological estimate. In contrast, the TACOS near-surface meridional velocities exhibit much larger variability relative to the climatology (Figure 2b). The largest meridional velocity signals occur during days 150–240 associated with the passage of three strong TIWs (amplitudes of 80 to 100 cm/s), followed by a period with weaker TIWs (amplitudes of 60 to 80 cm/s) in days 305–380. In days 262–287, just prior to the onset of the second series of TIWs, a series of superinertial (S.I.) oscillations is excited (amplitudes of 40 to 50 cm/s) with periods from 4 to 7 days (inertial period at 4°N is 7.1 days) concurrent with fluctuations in the mooring zonal and meridional winds (not shown).

The TACOS deployment was during a year with an anomalously warm eastern tropical Atlantic, one of the conditions that typically precedes a weak TIW season (e.g., Perez et al., 2012; Wu & Bowman, 2007). SST anomalies in the cold tongue region were quantified using ATL3 index defined as area-averaged SST anomalies from 20°W to 0° and from 3°S to 3°N (Figure 1; Zebiak, 1993). Summertime ATL3 anomalies estimated

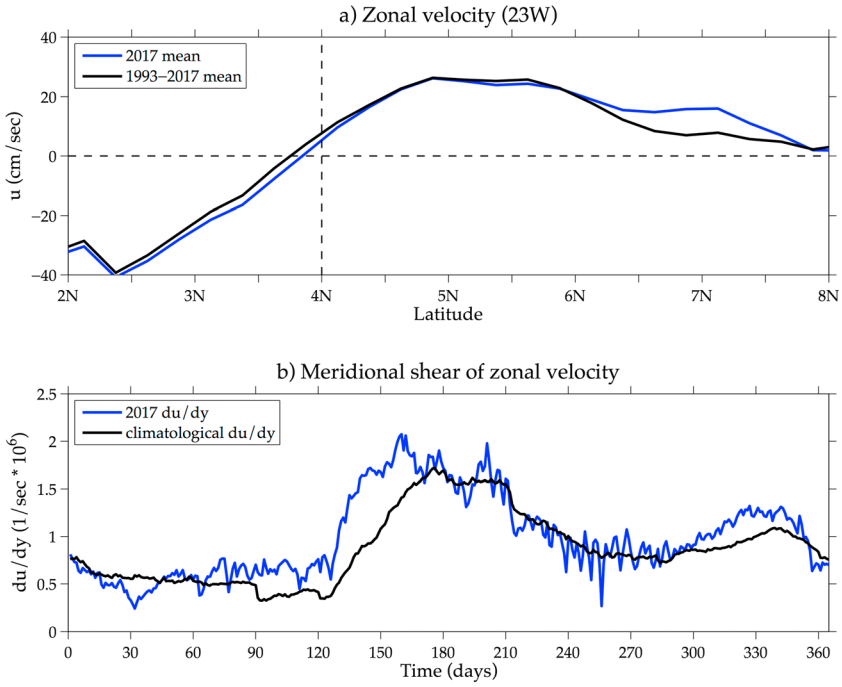

Figure 4. (a) Comparison of annual mean near-surface (15 m) zonal velocity along 23°W from the drifter-altimetry synthesis in 2017 (blue line) with the 1993-2017 mean (black line) as a function of latitude. (b) Comparison of the temporal evolution of meridional shear of zonal velocity (du/dy) in 2017 averaged between 3°N and 6°N and 30°W and 10°W (blue line) with the 1993-2017 climatological shear (black line).

from satellite SST were weak (approximately 0.3 °C) in 2017. Despite the weak cold tongue, it is clear that relatively strong TIW velocity fluctuations were measured (Figures 2b). The presence of TIWs can be easily confirmed through analysis of the satellite SST observations (Figure 3). Along 23°W, the TIWs produced the tell-tale cusp-shaped perturbations of the northern front of the Atlantic cold tongue in late spring/early summer and again in the fall (Figure 3a). Temporally and zonally band-pass filtered SST anomalies (20 to 50 day and 4° to 12° band pass, respectively, following Perez et al., 2012) show that SST perturbations greater than 0.2 °C in magnitude are often observed around 23°W (Figure 3b). When the instances of maximum 7-m depth northward velocity are overlaid onto the satellite SST plots (black dots in Figure 3), it is clear that the meridional velocity perturbations at the mooring are due to TIWs advecting relatively cold surface waters across the mooring.

The strength of the TIWs during the 2017 season can be quantified by applying a 20- to 50-day band-pass filter to the 10-m mooring temperature data and then computing the variance in a moving 4-month window (similar to the kinetic energy metric applied to mooring data in Perez et al., 2012). We find that the maximum 4-month TIW SST variance in the summer of 2017 (0.08 $°C^2$) was more than double the variance observed during the weak TIW conditions in 2016 (0.03 $°C^2$) and was nearly as large as the variance during the extremely energetic 2009 TIW season (0.10 $°C^2$) previously documented in Perez et al. (2012).

In addition to a strong cold tongue, another typical predictor for a strong off-equatorial TIW season is strong meridional SECN-NECC shear (e.g., Perez et al., 2012; von Schuckmann et al., 2008), which can be evaluated using the drifter-altimetry synthesis velocity data. Although the 2017 mean SECN (approximately -40 cm/s) and NECC (approximately 25 cm/s) were near the long-term (1993-2017) mean values along 23°W (Figure 4a), daily estimates of the meridional SECN-NECC shear in the vicinity of the mooring (averaged between 30° and 10°W and 3° and 6°N) show that the SECN-NECC shear was stronger than normal in late spring/early summer 2017 (Figure 4b), consistent with the observed energetic TIW season (Figures 2b and 3). Furthermore, the SECN-NECC shear in late 2017 also exceeded climatological shear values, consistent with the observed reemergence of TIWs during that time period (Figures 2b and 3).

3.2. Vertical Profiles of Velocity

The vertical structure of the mean and errors of TACOS velocities (red dots with lines in Figures 2c and 2d) are also compared to the means of zonal and meridional velocity generated from the combination of 36 shipboard/lowered ADCP casts, collected between March 1996 and August 2011 along 23°W, and a near-surface drifter and Argo float climatology (black lines and gray shading in Figures 2c and 2d, respectively), hereafter ADCP+D (Brandt et al., 2010; Perez et al., 2014). Note that Perez et al. (2014) focused exclusively on meridional velocities at 4°N, 23°W (see their Figure 9). Here, we show the concurrent zonal velocities in Figures 2c and 2d that were not discussed in that study.

The general vertical structure of mean zonal and meridional velocity and errors during the TACOS deployment (Figures 2c and 2d) mirrors the vertical structure of the ADCP+D means and standard errors, with almost northward flow at the surface that becomes increasingly northeastward between the surface and 25 m, shifting to southeastward flow below 25 m. During TACOS, the strongest mean zonal velocity is found at 37 m (9.9 cm/s; Table 1). After deriving the missing data at 37 m by vertical interpolation, we find similar mean eastward velocity of 8.6 cm/s (dashed red line in Figure 2c), suggesting that the subsurface maximum occurs at a depth between 32 and 47 m. Other than near the surface, the strongest mean meridional velocity (-3.6 $\pm$ 5.0 cm/s) is found at 57-m depth (Figure 2d). This value is nearly identical to the ADCP+D mean at the same depth, although the errors are large relative to the means. The mean horizontal velocity magnitude (or speed) is largest (29.2 cm/s) near the surface (Table 1) and decreases slowly with depth, despite the presence of subsurface maxima for the individual velocity components.

Mean speeds >20 cm/s persist down to 67 m and when combined with weak mean zonal and meridional velocities are indicative of the highly oscillatory flow captured during the TACOS deployment (Table 1). In addition, the observed meridional velocity fluctuations have much larger standard deviations than the zonal velocity fluctuations at all depths (Table 1; Figure 2). This differs from previous equatorial Atlantic studies, which have found that zonal velocity fluctuations dominate upper-ocean variability (Brandt et al., 2006; Weisberg et al., 1987) or are at most comparable to meridional velocity fluctuations (Grodsky et al., 2005; Weingartner & Weisberg, 1991; Wenegrat & McPhaden, 2015) on 10- to 100-day time scales.

3.3. Temporal-Vertical Variations of Horizontal Velocity and Vertical Shear

The energetic velocity perturbations inferred in the previous section are not confined to the surface, and for all depths, the meridional velocity fluctuations (Figure 5c) are stronger than their zonal velocity counterparts (Figure 5b; Table 1). During the first three TIWs (dashed vertical lines in Figure 5c), meridional velocities >60 cm/s penetrate down to 67-m depth, and perturbations as large as 40 cm/s are observed at 87 m before that sensor failed. Although weaker in amplitude, the S.I. oscillations and the fourth to sixth TIWs have velocity perturbations that reach to 57 and 67 m, respectively. Using lagged correlation analysis between the meridional velocity at 67 m and all other depths, vertical phase speeds of 14.4 and 12.6 m/day are estimated for the first and second set of TIWs, respectively (i.e., signals take 3 and 4 days to travel from 67 to 22 m). This upward vertical propagation was not observed during the S.I. oscillations.

Equatorial moorings have previously detected TIWs extending from the surface down to 80-120 m in the Atlantic (e.g., Grodsky et al., 2005; Weingartner & Weisberg, 1991; Weisberg & Weingartner, 1988; Wenegrat & McPhaden, 2015), but this is the first time they have been observed with such fine resolution at 4°N. Although not discussed in more recent studies (e.g., Grodsky et al., 2005; Wenegrat & McPhaden, 2015), upward phase propagation has previously been detected for TIWs at the equator in the Atlantic (e.g., Weisberg et al., 1980), consistent with the theoretical upward phase propagation and downward energy propagation for pure Rossby waves and mixed Rossby-gravity waves (e.g., Cox, 1980).

During TACOS, there is a tendency for negative vertical shear of zonal velocity (du/dz, eastward currents increasing with depth; Figure 2c) and positive vertical shear of meridional velocity (dv/dz, northward currents decreasing with depth; Figure 2d) above 40-50 m, and the opposite sign below (Figures 5c and 5d). However, du/dz, dv/dz, and the vertical shear of the total horizontal velocity squared vary dramatically over the TACOS record (Figures 5c, 5d, and 6a). Largest maximum shear squared values (~3×10^{-3} s^{-2}) are found in spring just before the first TIW arrives and in winter after the passage of the sixth TIW (black line, Figure 6a). There is modest total shear squared (~1 to 2×10^{-3} s^{-2}) during the passage of the TIWs and after the S.I. oscillations. Both du/dz and dv/dz contribute substantially to total vertical shear at all depths

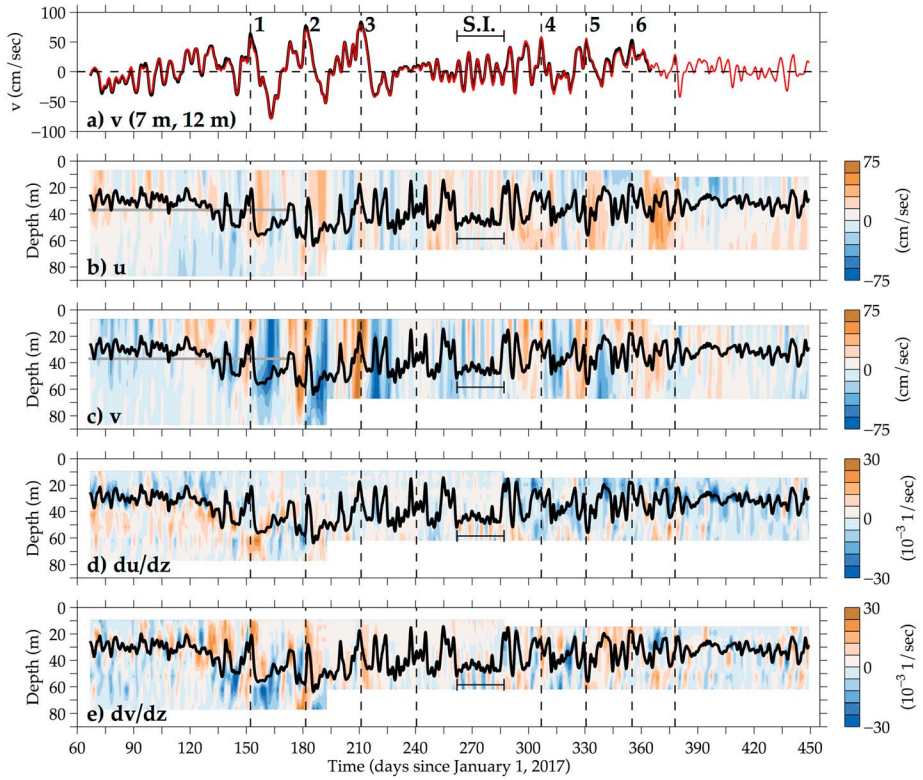

Figure 5. The 48-hr low-pass filtered time series of hourly (a) meridional velocity at 7-m (black line) and 12-m (red line) depth from Figure 2b. Tropical instability waves and superinertial (S.I.) events are denoted as in Figure 2b. Temporal-vertical evolution of (b) zonal and (c) meridional velocity, and vertical shear of (d) zonal and (e) meridional velocity. Thick black lines show the time series of the depth of maximum total shear squared. The gray lines at 37 m in panels (b) and (c) show the duration of the record at this depth.

(Figures 5d and 5e), and often the contribution of dv/dz to the total shear squared exceeds that of du/dz (red and blue lines in Figure 6a, respectively). This differs from the equator where du/dz associated with the westward SECN, and the underlying eastward flowing Equatorial Undercurrent dominates the total shear as seen in the Pacific during a TIW season (e.g., Inoue et al., 2012, 2019), and du/dz is often the only component documented in the equatorial Atlantic (e.g., Wenegrat & McPhaden, 2015).

The maximum shear squared depth (MSSD) also varies over the TACOS record (thick black line in Figures 5b–5e and 6b) and typically separates the negative du/dz and positive dv/dz near the surface from the underlying values of opposite sign (Figures 5d and 5e). We focus on the maximum shear squared rather than discussing the shear squared at the base of the mixed layer because during summer the mixed layer depth (MLD; computed from mooring temperature and salinity data using density criteria of 0.1 kg/m^3) can extend well past the vertical coverage of the TACOS instruments. The mean MSSD is 34 m, and the standard deviation is 11 m. In winter and spring (at the beginning and end of the record), the MSSD remains fairly steady at around 30 m. The MSSD is deepest during the maximum subsurface southward flow of the second TIW and shallowest during the maximum surface northward flow of the sixth TIW and before and after the S.I. oscillations (Figure 5c). During the S.I. oscillations themselves, the MSSD remains almost constant near 45 m. For most of the TIWs, a shallower (deeper) MSSD is seen during maximum northward (southward) flow. This is because southward flow typically penetrates deeper than the northward flow during a TIW, consistent with equatorial TIWs (Grodsky et al., 2005; Inoue et al., 2012, 2019; Wenegrat & McPhaden, 2015).

The MSSD exhibits weaker seasonal variability than the thermocline depth (Z20, blue line in Figure 6b), and the MSSD is always shallower than Z20. Temperature profiles are perturbed by the passage of the first three TIWs such that just after the maximum northward surface flow, Z20 deepens by 10 to 20 m (Figure 6b). After the maximum southward subsurface flow passes the mooring, Z20 shoals. During winter and spring, when

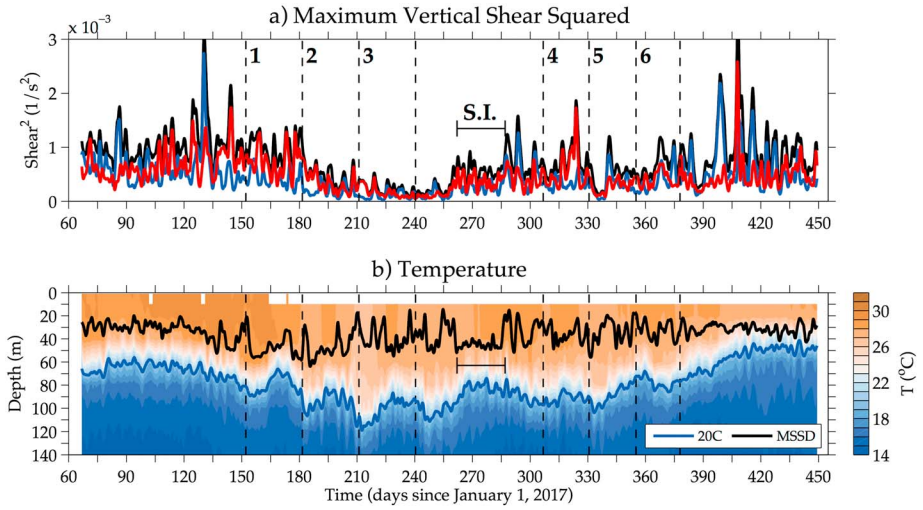

Figure 6. The 48-hr low-pass filtered time series of (a) the maximum vertical shear of horizontal velocity squared (black line) and the zonal (blue line) and meridional (red line) velocity contributions to the total shear squared, $(du/dz)^2$ and $(dv/dz)^2$, respectively. Tropical instability waves and superinertial (S.I.) events are denoted as in Figure 2b. Temporal-vertical evolution of 48-hr low-pass low-pass filtered (b) temperature, with the maximum shear squared depth (MSSD, black line) and Z20 (blue line) overlaid.

the MSSD is shallow, the MSSD is similar to the MLD (not shown). During summer, however, the MLD deepens and approaches the depth of the thermocline.

3.4. TIW Composite

Until now, TIW composites have not been generated for the tropical Atlantic. However, TIW composite analysis has been similarly applied to several months of moored data in the tropical Pacific at 2°N, 140°W influenced by the SECN and tropical cells (Cronin & Kessler, 2009) and at 0°N, 140°W influenced by the SECN and the Equatorial Undercurrent (Inoue et al., 2019). In addition, the velocity structure of a single equatorial TIW was studied in the Atlantic by Wenegrat and McPhaden (2015) and in the Pacific by Inoue et al. (2012), as well as the flow field of tropical instability vortices (TIVs) located to the north of the cold tongue front between TIW crests (Kennan & Flament, 2000; Menkes et al., 2002).

In this study, composites of horizontal velocity, shear, and temperature for the first three TIWs were created to examine the evolution of TIWs in a region influenced by the SECN and NECC and the tropical cells in more detail (Figure 7). The TIWs were aligned by the northward peak in surface flow (gray lines in Figure 7a). The period of the first two TIWs was 29.4 days. It was difficult to clearly delineate the termination of the third TIW, and therefore, a 29.4-day cutoff was also applied to that wave. The composite fields were not temporally filtered, although a time mean was removed at each depth. Composite anomalies are considered robust if the anomalies have the same sign for all three TIWs (marked by gray dots in Figures 7b–7e). Since the 87-m velocity sensor failed during passage of the second TIW, we exclude that depth from the composite analysis. As dv/dz exhibited larger variations than du/dz during the first three TIWs, we focus our composite analysis on the meridional shear component.

The TIW composite flow at 4°N, 23°W is asymmetric in time (Figure 7). For the first two days, there is anomalous northward flow between the surface and 67 m (Figure 7c). Then, an anomalous southward flow propagates upward and reaches the surface between days 4 and 12, with intermittent northward and southward flow between days 12 and 23. Later, northward flow propagates upward during the last 5 days to restart the TIW cycle. The first 10 days are characterized by anomalous eastward flow, after which there is anomalous westward flow, until the last 2 days of the cycle when the subsurface flow becomes eastward again (Figure 7b). The largest temperature anomalies (Figure 7e) are below 70 m, with strong subsurface warming (Z20 deepens, thick blue line) and weak surface cooling during the first 10 days and the last 5 days, and subsurface cooling (Z20 shoals) in between (days 10 to 25). In the composite TIW, dv/dz has large positive anomalies during the first 10 days in the upper 50–60 m (Figure 7d). Large negative dv/dz anomalies form

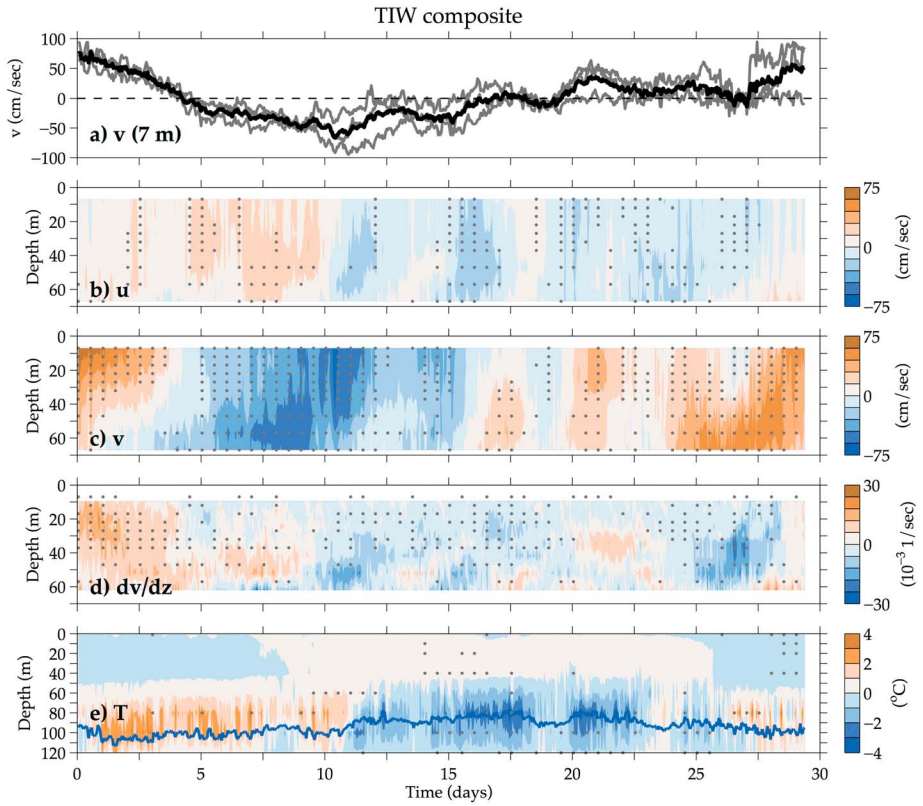

Figure 7. Composite based on the first 3 tropical instability waves (TIWs). Time zero corresponds the time of maximum northward surface flow. (a) Meridional velocity anomalies at 7 m for the first three TIWs (gray lines) and the composite (thick black line). Composite temporal-vertical evolution of (b) zonal and (c) meridional velocity, (d) vertical shear of meridional velocity, and (e) temperature anomalies. Gray dots show every 12 hr when the sign of the anomaly is the same for all three TIWs.

underneath around day 5, which later propagate upward (Figure 7d). During the last 5 days of the composite TIW, dv/dz has negative anomalies in the upper 60 m and positive anomalies that form underneath and begin to propagate upward (Figure 7e).

Whether the composite TIW flow is symmetric, and whether there is eastward or westward flow during the northward phase, depends on the latitude of the cold tongue front and the position and orientation of TIVs that form north of the cold tongue between successive TIWs (Cronin & Kessler, 2009; Hormann et al., 2013; Inoue et al., 2012, 2019; Kennan & Flament, 2000; Menkes et al., 2002; Wenegrat & McPhaden, 2015). For example, more symmetry would also be expected if the vortices crossed the mooring at their latitudinal mid-point and were longitudinally centered between successive TIWs. Altimetric sea surface height fields and inferred geostrophic velocity fields examined from 1993 to 2017 reveal high variability in the size, position, and orientation of the TIVs, although on average the center of the vortices passes close to 4°N (not shown). Instances where the northern portion of a TIV passes the mooring location and/or the TIV is tilted northeastward could yield the observed northeastward flow in the first few days of the composite. The composite TIW SST response is also location specific. Some studies find surface cooling (warming) during or just after the northward (southward) flow phase (Cronin & Kessler, 2009; Kennan & Flament, 2000; Menkes et al., 2002; Wenegrat & McPhaden, 2015), consistent with our study, whereas others find a less well-defined relationship, as other processes like surface heating can modulate temperatures within a TIW cycle (e.g., Inoue et al., 2012, 2019).

4. Larger-Scale Context of Observed Flow

Because the TACOS data analyzed here only elucidate the horizontal velocity and vertical shear structure at 4°N, 23°W during a 384-day time period, we use ancillary data (PIRATA mooring observations, ePIRATA,

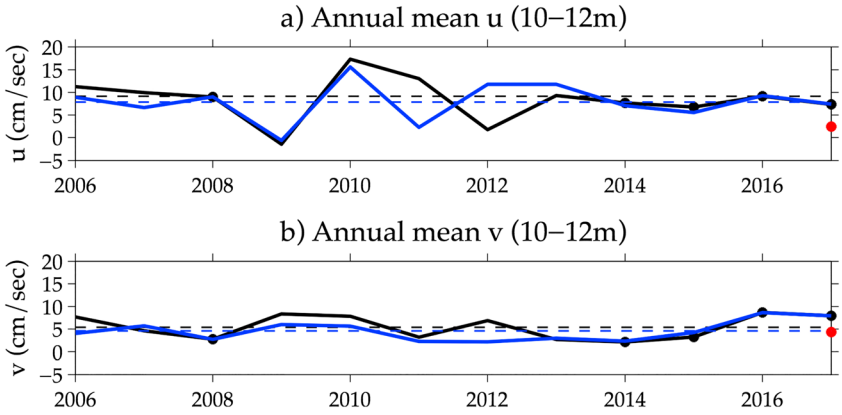

Figure 8. Time series of annual means of the combined 10-m (before March 2017) and 12-m (after March 2017) (a) zonal and (b) meridional velocity (black lines) at the 4°N, 23°W Prediction and Research Moored Array in the Tropical Atlantic (PIRATA) mooring. Black dots indicate years for which there are more than 8 months of mooring data. These values are compared with the enhanced PIRATA (ePIRATA) annual mean velocities (blue lines). Black and blue dashed lines represent the full record mean values for the PIRATA and ePIRATA, respectively. Red dots show the mean Tropical Atlantic Current Observations Study velocities at 12-m depth from March 2017 to March 2018.

drifter-altimetry synthesis) and output from reanalyses and numerical simulations to place those results within the larger context of the background tropical North Atlantic circulation.

4.1. Local Interannual Variability

Time series of annual mean near-surface velocities at 4°N, 23°W (black lines in Figures 8a and 8b) can be constructed using the combined long-term mooring velocity data at 10-m depth (before March 2017) and the recent observations at 12-m depth (after March 2017). In the merged mooring record, the 2017 mean near-surface zonal velocity at 4°N, 23°W (7.4 cm/s) was only slightly weaker than the 12-year mean zonal velocity (7.8 cm/s, black dashed line in Figure 8a). In addition, the 2017 mean meridional velocity (7.9 cm/s) was stronger than the 12-year mean meridional velocity (4.6 cm/s, black dashed line in Figure 8b). The larger 2017 mean compared to the TACOS period mean (red dots in Figures 8a and 8b) was due to the presence of a strong event with northeastward flow in early 2017 that occurred before the start of the TACOS experiment.

There can be large year-to-year differences in the near-surface annual mean velocities, with variations of ±8 cm/s in annual mean zonal velocity (Figure 8a) and ±4 cm/s in the annual mean meridional velocity (Figure 8b). It is important to note that the moored 10-m velocity data have many gaps in 2006-2007 and 2009-2013 when the largest interannual variability of zonal (and to a lesser extent meridional) velocity is observed (black dots in Figure 8 indicate when annual record gaps are shorter than 4 months). In more recent (and better sampled) years, 2014-2017, there is less interannual variability. To reduce the potential of seasonal aliasing due to these temporal gaps, the seasonal cycles of near-surface zonal and meridional velocity were removed prior to computing the annual means. However, given the lack of a strong seasonal cycle (gray lines in Figures 2a and 2b), it is possible that some aliasing still remains.

To examine this further, we also computed annual mean 10-m velocities from the continuous-in-time ePIRATA data set (blue lines in Figure 8). As expected, ePIRATA estimates of the annual mean zonal and meridional velocities agree best with the mooring estimates during years when there is good mooring data coverage (compare blue and black lines), and the long-term means are very similar (compare blue and black dashed lines). Furthermore, ePIRATA annual means provide added confirmation that the year-to-year variations of mean zonal velocity in 2013-2017 were weaker than those observed earlier in 2009-2012.

Analysis of the drifter-altimetry synthesis velocities at 15-m depth shows even larger interannual variability from 1993 to 2017, with annual mean zonal velocities varying from -2 to 13 cm/s at 4°N, 23°W (black line in Figure 9a). Near-surface zonal and meridional velocity interannual variations are predominantly buoyancy driven (red lines in Figure 9, geostrophic contribution) rather than wind driven (blue line in Figure 9, Ekman contribution). The drifter-altimetry synthesis record also shows that near-surface zonal velocity

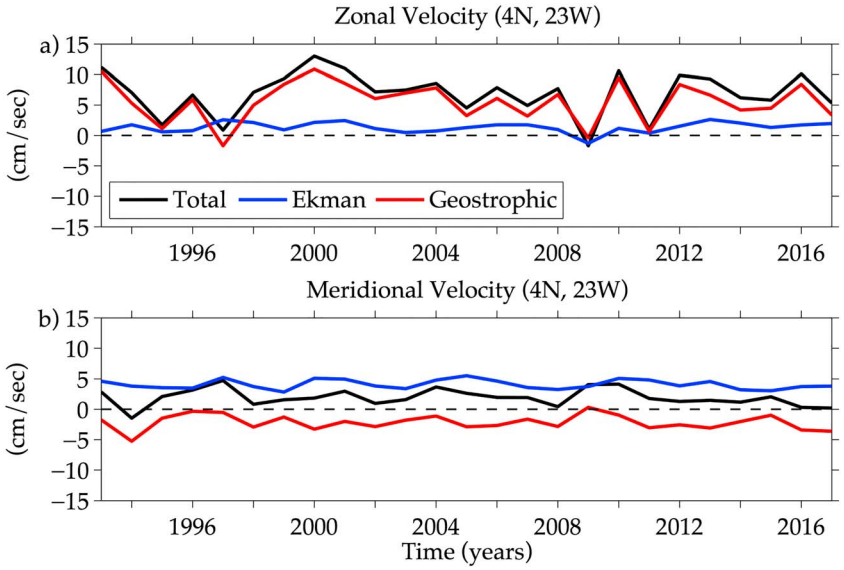

Figure 9. Time series of annual mean near-surface, 15 m, (a) zonal and (b) meridional velocities from the drifter-altimetry synthesis at 4°N, 23°W (black lines). Blue and red lines show the Ekman and geostrophic velocity contributions, respectively.

exhibits larger interannual variability from 1993 to 2000 and from 2009 to 2012 compared to the early 2000s and more recent years (2013-2017).

Given the lack of subsurface velocity observations prior to TACOS, the only way to explore the interannual variability of velocity in the upper 100 m is to look at numerical models (OFES; Figures 10c and 10f) and reanalysis products (ORAS4 and GODAS, Figures 10a and 10d, and 10b and 10e, respectively). The annual mean zonal velocities exhibit ±10 cm/s interannual variations from the surface down to 100 m (gray lines in Figures 10a–10c), with less variability (±5 cm/s) in the annual mean meridional velocities (Figures 10d–10f). The simulated velocity progresses from northeastward at the surface to southeastward below 20 to 30 m, with largest mean zonal velocity between 30 and 40 m and largest mean meridional velocity between 40 and 60 m. The interannual variability is highest near the surface, especially for zonal velocity. Overlaying the TACOS mean and standard errors onto the model profiles (red dots with horizontal lines in Figure 10), we see that the observed mean meridional velocity profile agrees quite well with the range of simulated annual mean meridional velocities and often overlaps with the long-term mean within the observed uncertainty (Figures 10d–10f). The observed mean zonal velocity profile rarely overlaps with the simulated long-term mean zonal velocity, though it mostly does fall within range of possible annual mean zonal velocities in ORAS4 and GODAS (Figures 10a and 10b). This suggests that a long observational record will be needed to produce a robust estimate of the background mean zonal velocity at 4°N, 23°W suitable to validate numerical models.

4.2. Influences of Large-Scale Circulation on Interannual Variability

These results immediately prompt the question: What changes in the large-scale tropical circulation control the interannual variability of zonal velocity at 4°N, 23°W in the real ocean and the models? As mentioned earlier, the mooring is situated just north of the mean SECN-NECC boundary (Figure 1). In addition to the SECN-NECC boundary shifting closer to the mooring in 2017 (e.g., Figure 4a), the NECC core shifting further northward, or the NECC weakening could also produce weaker eastward flow at 4°N, 23°W.

From the drifter altimetry-synthesis data between 1993 and 2017 (Figure 11a), it is clear that the annual mean peak velocity of the NECC along 23°W (defined as the maximum 15-m eastward velocity between 2.5°N and 9°N in the daily fields and then annually averaged, blue line) is related to the annual mean 15-m zonal velocity observed at 4°N, 23°W (black line) with a modest correlation of $r = 0.47$ that is significant at the 95% level (large black dot in Figure 12). In other words, a weaker (stronger) NECC often corresponds to weaker (stronger) eastward flow at the mooring. This relationship depends on the proximity of

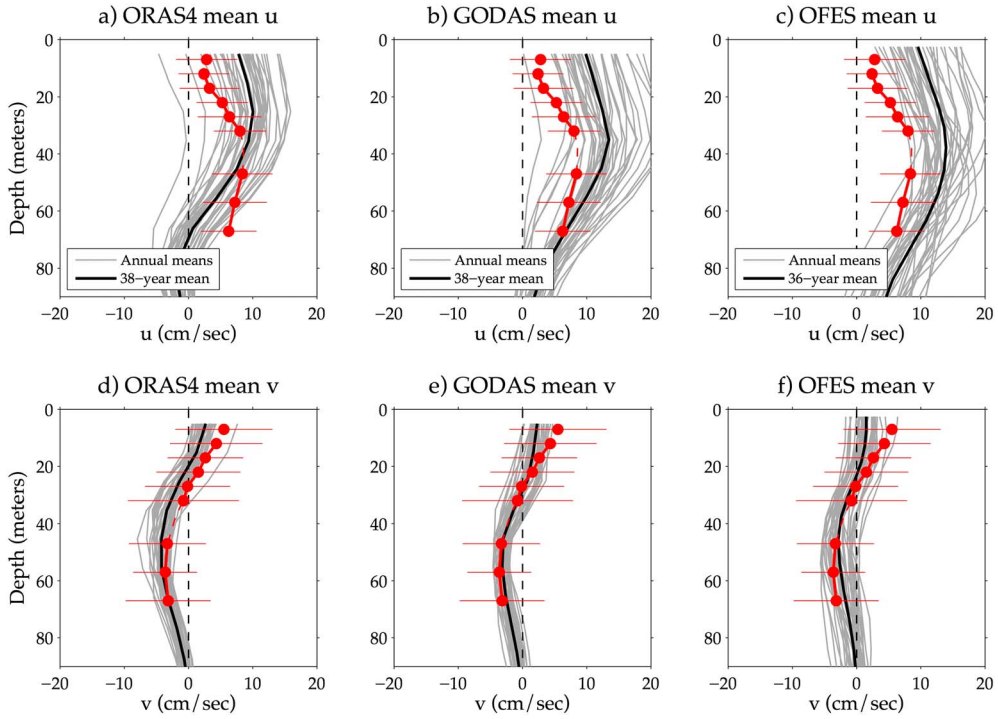

Figure 10. Vertical profiles of annual mean (a–c) zonal and (d–f) meridional velocity (gray lines) and long-term means (black lines) for ocean reanalysis system 4 (ORAS4) and global ocean data assimilation system (GODAS) reanalyses and the Ocean general circulation model for the Earth Simulator (OFES) simulation at 4°N, 23°W. Tropical Atlantic Current Observations Study (TACOS) record means and errors from Figures 2c and 2d are overlaid in red.

the NECC to the mooring. When the NECC is displaced southward (blue line in Figure 11b), its strength is more closely related to the zonal velocity at the mooring, and we find that the NECC core latitude and zonal velocity at 4°N are anticorrelated (r = -0.52, significant at 95%). However, the largest influence on the eastward velocity at 4°N, 23°W is exerted by the latitude of the SECN-NECC boundary along 23°W

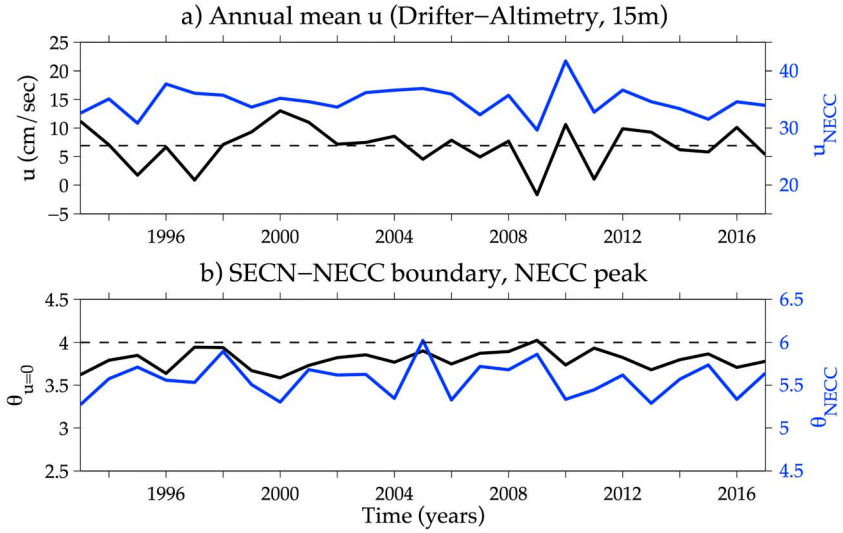

Figure 11. Time series of (a) annual mean near-surface (15 m) zonal velocity at 4°N, 23°W from the total drifter-altimetry synthesis (black line, same record as in Figure 9a) compared with the mean peak NECC zonal velocity along 23°W (U_{NECC}, blue line). Time series of (b) annual mean latitude along 23°W of the SECN-NECC boundary ($\theta_{u=0}$, black line) and latitude of the peak NECC zonal velocity (θ_{NECC}, blue line). Note y axis on the right side corresponds to blue curves. NECC = North Equatorial Countercurrent; SECN = northern branch of South Equatorial Current.

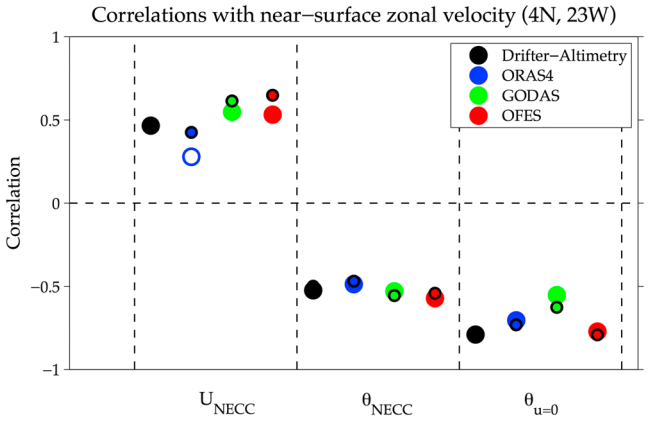

Figure 12. Correlations between annual mean zonal velocity at 4°N, 23°W with the annual mean peak NECC core zonal velocity (U_{NECC}), mean latitude of NECC core (θ_{NECC}), and mean latitude of SECN-NECC boundary ($\theta_{u=0}$) along 23°W. Large symbols correspond to full-record correlations (see section 2), while smaller symbols correspond to correlations for the period of overlap (1993-2015). Dots (open circles) show correlations that are significant (insignificant) with 95% confidence. Additional statistics are provided in Table 2. NECC = North Equatorial Countercurrent; SECN = northern branch of South Equatorial Current; ORAS4 = ocean reanalysis system 4; GODAS = global ocean data assimilation system; OFES = Ocean general circulation model for the Earth Simulator.

(defined as the latitude where zonal velocity is zero between 1.5°N and the NECC core latitude). This latitude is typically less than 0.4° south of the mooring, sometimes overlapping the mooring latitude (black line in Figure 11b), and is anticorrelated with the zonal velocity at the mooring (r = -0.79, significant at 95%). During 2017, the NECC core velocity was approximately 34.0 cm/s (0.7 cm/s weaker than the long-term mean) and located at 5.6°N (less than 0.1° north of the long-term mean position), and the SECN-NECC boundary was at 3.8°N (close to the mooring location and equal to the long-term mean position). All three factors are consistent with the slightly weaker mean zonal velocity at 4°N, 23°W in 2017 compared to the longer-term mean.

Next, we examine the extent to which these relationships are present in the models. Table 2 summarizes the mean values of near-surface zonal velocity at 4°N, 23°W, the NECC core strength and latitude along 23°W, and the latitude of the SECN-NECC boundary along 23°W for the drifter-altimetry synthesis, the OFES model, and the two reanalysis products. Values are only discussed for the common period of overlap 1993-2015, but the full-record means are very similar and provided in Table 2. Note that the uppermost velocity depth is 5 m for ORAS4 and GODAS and 2.5 m for OFES.

The 1993-2015 mean near-surface zonal velocities at 4°N, 23°W agree best between ORAS4 and the drifter-altimetry synthesis (6.6 and 6.8 cm/s, respectively) with slightly stronger mean flow observed in GODAS and OFES (10.4 and 9.7 cm/s, respectively). All of the models have weaker mean NECC velocities (20.9 to 27.2 cm/s) than the drifter altimetry synthesis (about 35 cm/s). ORAS4 and OFES place the mean position of the NECC core (5.7°N and 5.5°N, respectively) nearest to the observed mean position (5.6°N), whereas in GODAS it is at 5.1°N. The observed 1993-2015 mean latitude of the SECN-NECC boundary is just south of the TACOS mooring at 3.8°N. The models all place the SECN-NECC boundary south of the mooring, with ORAS4 and OFES nearest to the mooring (3.5°N) and GODAS furthest south (3.1°N).

Given this proximity of the SECN-NECC boundary to the latitude of the mooring, the near-surface zonal velocity at 4°N, 23°W systematically shows the strongest anticorrelation between the position of the SECN-NECC boundary and the flow at 4°N, 23°W in the models and drifter-altimetry synthesis (Figure 12). During the common period of overlap (small dots on Figure 12), these anticorrelations are -0.63 (GODAS), -0.79 (OFES), -0.73 (ORAS4), and -0.79 (drifter-altimetry synthesis) and are all significant with 95% confidence. There is generally modest but significant anticorrelation between the zonal velocity at 4°N, 23°W and the latitude of the NECC core (between -0.45 and -0.55), and this relationship is strongest

Table 2
Mean and standard deviation (σ) of annual averages of zonal velocity at 4°N, 23°W, NECC peak zonal velocity and latitude along 23°W, and the latitude of the SECN-NECC boundary (u=0) along 23°W for the full time period available for each product, and for the common time period of overlap 1993 to 2015

Product	Time period	Mean (σ) u (cm/s) 4N, 23W	Mean (σ) NECC core u (cm/s)	Mean (σ) NECC core latitude	Mean (σ) u=0 latitude
Drifter altimetry	1993-2017	6.9 (3.6)	34.7 (2.5)	5.6° (0.2°)	3.8° (0.1°)
	1993-2015	6.8 (3.7)	34.8 (2.6)	5.6° (0.2°)	3.8° (0.1°)
ORAS4	1980-2017	7.8 (3.9)	21.9 (3.2)	5.6° (0.5°)	3.4° (0.3°)
	1993-2015	6.6 (3.9)	22.6 (3.5)	5.7° (0.5°)	3.5° (0.3°)
GODAS	1980-2017	9.9 (4.1)	19.6 (3.7)	5.1° (0.4°)	3.1° (0.3°)
	1993-2015	10.4 (4.8)	20.9 (3.2)	5.1° (0.5°)	3.1° (0.3°)
OFES	1980-2015	9.5 (4.1)	26.4 (4.2)	5.5° (0.4°)	3.5° (0.3°)
	1993-2015	9.7 (4.3)	27.2 (4.6)	5.5° (0.4°)	3.5° (0.4°)

Note. NECC = North Equatorial Countercurrent; SECN = northern branch of South Equatorial Current; ORAS4 = ocean reanalysis system 4; GODAS = global ocean data assimilation system; OFES = Ocean general circulation model for the Earth Simulator.

in GODAS and OFES. Despite the NECC being north of the mooring in the models and the drifter-altimetry synthesis, the positive correlation between the NECC core velocity and zonal velocity at the mooring is still considerable and significant (between 0.42 and 0.65) during the common period of overlap.

5. Summary, Conclusions, and Implications for Future Observations

TACOS sampled hourly upper ocean currents and vertical shear from a mooring at 4°N, 23°W in the tropical North Atlantic for the first time. Analysis of the first 384 days of TACOS data, collected between March 2017 and March 2018, has yielded several new insights. During this time, the mean zonal velocity and vertical shear were strongest between 32 and 37 m, and near-surface mean eastward currents were weaker than the long-term 10-m mean eastward currents. The ocean model and reanalyses examined here support the existence of subsurface extrema in zonal and meridional velocity compared to surface values, and analysis of the long-term mooring and ePIRATA velocity data finds that the TACOS near-surface mean velocities were indeed weak relative to the 2017 means because a strong northeastward flow event was missed in early 2017. Continuous measurements are important in this region, as missed intraseasonal variability due to temporal gaps in the data can alias annual means. In addition, substantial interannual variability of near-surface zonal velocity can be expected at 4°N, 23°W, requiring multiple years of observations to produce a robust long-term mean velocity profile. Based on the observational and model analysis, this interannual zonal velocity variability is predominantly geostrophic and is strongly influenced by the latitudinal distance between the SECN-NECC boundary and the mooring (although the strength and latitude of the NECC core can also be important).

Preliminary analysis of the relationship between the interannual zonal velocity variability at 4°N, 23°W and dominant coupled ocean-atmosphere modes in the tropical Atlantic (e.g., Chiang & Vimont, 2004; Zebiak, 1993) was conducted using satellite SST data from 1998 to 2017. The summertime ATL3 SST index was used a proxy for the strength of the Atlantic zonal mode, and the differences between spring SST anomalies in the region 3°N to 20°N, 60°W to 15°E minus those in the region 10°S to 3°N and 60°W to 15°E (Rugg et al., 2016) were used as a proxy for the strength of the Atlantic meridional mode. Although Hormann et al. (2012) found that the strength and position of the NECC peak depend on the tropical Atlantic coupled modes, these modes do not fully explain the zonal velocity variability at 4°N, 23°W. We found weak correlations (0.15 to 0.35) between interannual zonal velocity variability at 4°N, 23°W and the tropical Atlantic coupled modes from 1998 to 2017. However, these correlations increase to 0.58-0.65 over the last decade, with stronger annual zonal velocity during years of positive zonal and meridional modes. The causes of these decadal changes should be studied further in future analyses.

Energetic TIWs were observed in 2017 in horizontal velocity, vertical shear, and temperature at 4°N, 23°W despite the anomalously warm cold tongue, which is one of the conditions that typically precede a weak TIW season (e.g., Perez et al., 2012; Wu & Bowman, 2007). Analysis of drifter-altimetry synthesis data between 3°N and 6°N demonstrated that the SECN-NECC shear was slightly stronger than climatological values in early summer and late fall 2017, consistent with the generation of an energetic TIW season in the summer and the subsequent re-emergence of TIWs in the fall.

Despite large meridional velocity fluctuations associated with TIWs that extended down to 87 m, only modest vertical shears were observed during the TIWs compared to shear measured in spring 2017 before the first set of TIWs, and in winter 2018 after the second set of TIWs. If vertical mixing is shear driven, this suggests TIWs may be less crucial for vertical turbulent cooling at 4°N, 23°W than they are near the equator (Hummels et al., 2013, 2014). TIW velocity fluctuations did, however, perturb both the thermocline and the depth of maximum vertical shear squared. TIW velocity fluctuations also propagated upward with vertical phase speeds of 12-15 m/day. Coherent velocity, vertical shear, and temperature variations were found in a composite TIW, such that the composite began with northeastward flow and large positive vertical shear of meridional velocity (dv/dz) in the upper 50 to 60 m with southwestward flow and negative dv/dz underneath, which preceded strong subsurface warming below 70 m.

The TACOS velocity and shear data set provide a unique and valuable resource for assessing model skill in the tropical North Atlantic on high temporal and vertical scales. While we have focused on daily and longer time scales in this study, we note that the unfiltered maximum vertical shear squared values (gray line in Figure 13a) greatly exceed the 48-hr low-pass filtered values (black line in Figure 13a). The large shear

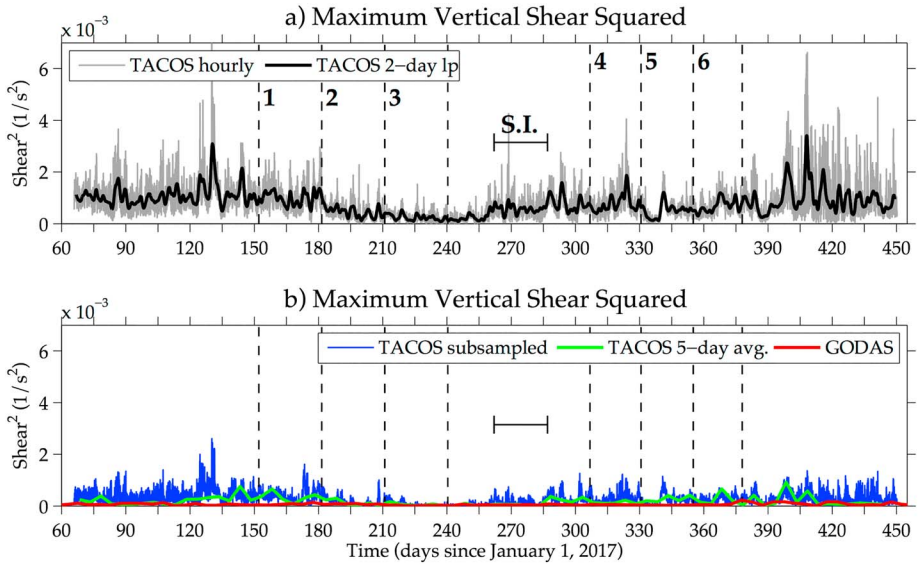

Figure 13. (a) Comparison of hourly maximum total shear squared from Tropical Atlantic Current Observations Study (TACOS; gray line) and 2-day low-pass filtered values (black line repeated from Figure 6a). (b) Comparison of maximum shear squared computed from 5-day averages of TACOS velocities (green line), and from the vertically subsampled hourly TACOS velocities (blue line) discussed in section 5. The red line shows the maximum shear squared values computed from global ocean data assimilation system (GODAS) 5-day mean velocities, respectively. Note that the range of the *y* axis is larger in the top panel.

squared values are further reduced when computed from 5-day averages of the observed velocity (green line in Figure 13b, note *y* axis scale changes). Numerical models and reanalyses typically output fields at several days to monthly increments (e.g., GODAS 5-day averages, red line in Figure 13b). To fully validate these models in the future, it will be necessary to access hourly to daily fields to better assess whether they are able to accurately simulate high-frequency variations in horizontal velocity and vertical shear.

A subset of the TACOS point acoustic current meters were redeployed in March 2018 nominally at 27-, 37-, 57-, and 87-m depths, as part of TACOS-2, as well as the standard 12-m point acoustic current meter. Preliminary analysis of these data, relayed in real time via Iridium satellites, suggests that regardless of year-to-year differences, this reduced TACOS-2 configuration will miss a significant portion of the fine-scale vertical shear captured in the first year. This can be illustrated by vertically subsampling the first year of TACOS velocity data to those five depths. This subsampling causes the amplitude of the high-frequency maximum vertical shear squared values to drop considerably (compare blue line in Figure 13b with gray line in Figure 13a) and suggests that fine vertical sampling (less than 10 m) is needed to observe intense vertical shear events in this region. A more detailed analysis of the impact of high-frequency and fine-vertical scale vertical shear variations on estimating turbulent mixing, vertical heat fluxes, and closing the heat budget at 4°N, 23°W, as well as comparisons between the first year and subsequent deployments, will be the subject of future study.

Acknowledgments
The authors thank Sang-Ki Lee, Silvia Garzoli, Libby Johns, and Gustavo Goni for insightful comments on an early draft of the manuscript. Thank you to the ship captains and crew who have supported PIRATA Northeast Extension (PNE) research cruises. We also thank the administrative, support, and technical teams in Miami, FL and Seattle, WA who helped develop the plan for TACOS; prepare, deploy, and recover the TACOS instruments; and collect and transmit the real-time data. We specifically acknowledge Gustavo Goni, Grant Rawson, Ulises Rivero, Shaun Dolk, Erik Valdes, Libby Johns, Ryan Smith, Chris Meinen, Jonathan Christophersen (Miami team); Michael McPhaden, Kenneth Connell, Paul Freitag, Steven Kunze, and Ryan Wells (Seattle team). The authors were supported by NOAA's Ocean Observing and Monitoring Division (Funding Reference 100007298) and the Atlantic Oceanographic and Meteorological Laboratory (AOML). AOML's Physical Oceanography Division provided support for TACOS instrument acquisition. More information about the PNE program can be found at the NOAA/AOML website (www.aoml.noaa.gov/phod/pne/). PIRATA and TACOS data can be found at the NOAA Pacific Marine Environmental Laboratory (PMEL) website (https://www.pmel.noaa.gov/gtmba/pirata).

References

Balmaseda, M. A., Mogensen, K., & Weaver, A. T. (2013). Evaluation of the ECMWF ocean reanalysis system ORAS4. *Quarterly Journal of the Royal Meteorological Society*, *139*(674), 1132–1161. https://doi.org/10.1002/qj.2063

Behringer, D., & Xue, Y. (2004). Evaluation of the global ocean data assimilation system at NCEP: The Pacific Ocean. Preprints, Eighth Symp. on Integrated Observing and Assimilation Systems for Atmosphere, Oceans, and Land Surface, Seattle, WA, Amer. Meteor. Soc., 2.3. Retrieved from https://ams.confex.com/ams/pdfpapers/70720.pdf

Bourlès, B., Araujo, M., McPhaden, M. J., Brandt, P., Foltz, G. R., Lumpkin, R., et al. (2019). PIRATA: A sustained observing system for tropical Atlantic climate research and forecasting. *Earth and Space Science*, *6*, 577–616. https://doi.org/10.1029/2018EA000428

Bourlès, B., Lumpkin, R., McPhaden, M. J., Hernandez, F., Nobre, P., Campos, E., et al. (2008). The PIRATA Program: History, accomplishments, and future directions. *Bulletin of the American Meteorological Society*, *89*(8), 1111–1126. https://doi.org/10.1175/2008BAMS2462.1

Brandt, P., Caniaux, G., Bourlès, B., Lazar, A., Dengler, M., Funk, A., et al. (2011). Equatorial upper-ocean dynamics and their interaction with the West African Monsoon. *Atmospheric Science Letters*, *12*(1), 24–30. https://doi.org/10.1002/asl.287

Brandt, P., Funk, A., Tantet, A., Johns, W. E., & Fischer, J. (2014). The Equatorial Undercurrent in the central Atlantic and its relation to tropical Atlantic variability. *Climate Dynamics*, *43*(11), 2985–2997. https://doi.org/10.1007/s00382-014-2061-4

Brandt, P., Hormann, V., Bourlès, B., Fischer, J., Schott, F. A., Stramma, L., & Dengler, M. (2008). Oxygen tongues and zonal currents in the equatorial Atlantic. *Journal of Geophysical Research*, *113*, C04012. https://doi.org/10.1029/2007JC004435

Brandt, P., Hormann, V., Körtzinger, A., Visbeck, M., Krahmann, G., Stramma, L., et al. (2010). Changes in the ventilation of the oxygen minimum zone of the tropical North Atlantic. *Journal of Physical Oceanography*, *40*(8), 1784–1801. https://doi.org/10.1175/2010JPO4301.1

Brandt, P., Schott, F. A., Provost, C., Kartavtseff, A., Hormann, V., Bourlès, B., & Fischer, J. (2006). Circulation in the central equatorial Atlantic: Mean and intraseasonal to seasonal variability. *Geophysical Research Letters*, *33*, L07609. https://doi.org/10.1029/2005GL025498

Burmeister, K., Brandt, P., & Lübbecke, J. F. (2016). Revisiting the cause of the eastern equatorial Atlantic cold event in 2009. *Journal of Geophysical Research: Oceans*, *121*, 4777–4789. https://doi.org/10.1002/2016JC011719

Caltabiano, A. C. V., Robinson, I. S., & Pezzi, L. P. (2005). Multi-year satellite observations of instability waves in the tropical Atlantic Ocean. *Ocean Science Discussions*, *2*(1), 1–35. https://doi.org/10.5194/osd-2-1-2005

Chiang, J. C. H., & Vimont, D. J. (2004). Anomalous Pacific and Atlantic meridional modes of tropical atmospheric-ocean variability. *Journal of Climate*, *17*(21), 4143–4158. https://doi.org/10.1175/JCLI4953.1

Cox, M. (1980). Generation and propagation of 30-day waves in a numerical model of the Pacific. *Journal of Physical Oceanography*, *10*(8), 1168–1186. https://doi.org/10.1175/1520-0485(1980)010<1168:GAPODW>2.0.CO;2

Cronin, M. F., & Kessler, W. S. (2009). Near-surface shear flow in the tropical Pacific cold tongue front. *Journal of Physical Oceanography*, *39*(5), 1200–1215. https://doi.org/10.1175/2008JPO4064.1

Foltz, G. R., Grodsky, S. A., Carton, J. A., & McPhaden, M. J. (2003). Seasonal mixed layer heat budget of the tropical Atlantic Ocean. *Journal of Geophysical Research*, *108*(C5), 3146. https://doi.org/10.1029/2002JC001584

Foltz, G. R., McPhaden, M. J., & Lumpkin, R. (2012). A strong Atlantic Meridional Mode event in 2009: The role of mixed layer dynamics. *Journal of Climate*, *25*(1), 363–380. https://doi.org/10.1175/JCLI-D-11-00150.1

Foltz, G. R., Schmid, C., & Lumpkin, R. (2018). An enhanced PIRATA data set for tropical Atlantic ocean-atmosphere research. *Journal of Climate*, *31*(4), 1499–1524. https://doi.org/10.1175/JCLI-D-16-0816.1

Garzoli, S. G., & Katz, E. J. (1984). The forced annual reversal of the Atlantic North Equatorial Countercurrent. *Journal of Physical Oceanography*, *13*, 2082–2090.

Garzoli, S. L., Dong, S., Fine, R., Meinen, C. S., Perez, R. C., Schmid, C., et al. (2015). The fate of the deep western boundary current in the South Atlantic. *Deep Sea Research, Part I*, *103*, 125–136. https://doi.org/10.1016/j.dsr.2015.05.008

Goes, M., Goni, G. J., Hormann, V., & Perez, R. C. (2013). Variability of the Atlantic off-equatorial eastward currents during 1993-2010 using a synthetic method. *Journal of Geophysical Research: Oceans*, *118*, 3026–3045. https://doi.org/10.1002/jgrc.20186

Goldenberg, S. B., & Shapiro, L. J. (1996). Physical mechanisms for the association of El Niño and West African rainfall with major hurricane activity. *Journal of Climate*, *9*(6), 1169–1187. https://doi.org/10.1175/1520-0442(1996)009<1169:PMFTAO>2.0.CO;2

Grodsky, S. A., Carton, J. A., Provost, C., Servain, J., Lorenzzetti, J. A., & McPhaden, M. J. (2005). Tropical instability waves at 0°N, 23°W in the Atlantic: A case study using Pilot Research Moored Array in the Tropical Atlantic (PIRATA) mooring data. *Journal of Geophysical Research*, *110*, C08010. https://doi.org/10.1029/2005JC002941

Helber, R. W., Weisberg, R. H., Bonjean, F., Johnson, E. S., & Lagerloef, G. S. E. (2007). Satellite-derived surface current divergence in relation to tropical Atlantic SST and wind. *Journal of Physical Oceanography*, *33*, 1357–1375.

Hormann, V., Lumpkin, R., & Foltz, G. (2012). Interannual North Equatorial Countercurrent variability and its relation to tropical Atlantic climate Modes. *Journal of Geophysical Research*, *117*, C04035. https://doi.org/10.1029/2011JC007697

Hormann, V., Lumpkin, R., & Perez, R. C. (2013). A generalized method for estimating the structure of the equatorial Atlantic cold tongue: application to drifter observations. *Journal of Atmospheric and Oceanic Technology*, *30*(8), 1884–1895. https://doi.org/10.1175/JTECH-D-12-00173.1

Hummels, R., Dengler, M., & Bourlès, B. (2013). Seasonal and regional variability of upper ocean diapycnal heat flux in the Atlantic Cold Tongue. *Progress in Oceanography*, *111*, 52–74. https://doi.org/10.1016/j.pocean.2012.11.001

Hummels, R., Dengler, M., Brandt, P., & Schlundt, M. (2014). Diapycnal heat flux and mixed layer heat budget within the Atlantic Cold Tongue. *Climate Dynamics*, *43* (11), 3179–3199. http://dx.doi.org/10.1007/s00382-014-2339-6

Inoue, R., Lien, R.-C., & Moum, J. N. (2012). Modulation of equatorial turbulence by a tropical instability wave. *Journal of Geophysical Research*, *117*, C10009. https://doi.org/10.1029/2011JC007767

Inoue, R., Lien, R.-C., Moum, J. N., Perez, R. C., & Gregg, M. C. (2019). Variations of equatorial shear, stratification, and turbulence within a tropical instability wave cycle. *Journal of Geophysical Research: Oceans*, *124*, 1858–1875. https://doi.org/10.1029/2018JC014480

Johns, W. E., Brandt, P., Bourlès, B., Tantet, A., Papapostolou, A., & Houk, A. (2014). Zonal structure and seasonal variability of the Atlantic Equatorial Undercurrent. *Climate Dynamics*, *43*(11), 3047–3069. https://doi.org/10.1007/s00382-014-2136-2

Kennan, S., & Flament, P. (2000). Observations of a tropical instability vortex. *Journal of Physical Oceanography*, *30*(9), 2277–2301. https://doi.org/10.1175/1520-0485(2000)030<2277:OOATIV>2.0.CO;2

Kersalé, M., Perez, R. C., Speich, S., Meinen, C. S., Lamont, T., Le Hénaff, M., et al. (2019). Shallow and deep eastern boundary currents in the South Atlantic at 34.5°S: Mean structure and variability. *Journal of Geophysical Research: Oceans*, *124*, 1634–1659. https://doi.org/10.1029/2018JC014554

Kossin, J. P., & Vimont, D. J. (2007). A more general framework for understanding Atlantic hurricane variability and trends. *Bulletin of the American Meteorological Society*, *88*(11), 1767–1782. https://doi.org/10.1175/BAMS-88-11-1767

Laurindo, L. C., Mariano, A., & Lumpkin, R. (2017). An improved surface velocity climatology for the global ocean from drifter observations. *Deep-Sea Research Part I*, *124*, 73–92. https://doi.org/10.1016/j.dsr.2017.04.009

Lubbecke, J. F. (2013). Tropical Atlantic warm events. *Nature Geoscience*, *6*(1), 22–23. https://doi.org/10.1038/ngeo1685

Lumpkin, R., & Garzoli, S. (2011). Interannual to decadal changes in the western South Atlantic's surface circulation. *Journal of Geophysical Research*, *116*, C01014. https://doi.org/10.1029/2010JC006285

Lumpkin, R., & Garzoli, S. L. (2005). Near-surface circulation in the tropical Atlantic Ocean. *Deep-Sea Research Part I*, *52*(3), 495–518. https://doi.org/10.1016/j.dsr.2004.09.001

Lumpkin, R., & Johnson, G. C. (2013). Global ocean surface velocities from drifters: Mean, variance, El Nino-Southern Oscillation response, and seasonal cycle. *Journal of Geophysical Research: Oceans*, *118*, 2992–3006. https://doi.org.10.1002/jgrc.20210

Masumoto, Y., Sasaki, H., Kagimoto, T., Komori, N., Ishida, A., Sasai, Y., et al. (2004). A fifty-year eddy-resolving simulation of the world ocean—Preliminary outcomes of OFES (OGCM for the Earth Simulator). *Journal of the Earth Simulator*, *1*, 35–56.

Meinen, C. S., Garzoli, S. L., Perez, R. C., Campos, E., Piola, A. R., Chidichimo, M.-P., et al. (2017). Characteristics and causes of Deep Western Boundary Current transport variability at 34.5°S during 2009-2014. *Ocean Science*, *13*(1), 175–194. https://doi.org/10.5194/os-13-175-2017

Menkes, C. E., Kennan, S. C., Flament, P., Dandonneau, Y., Masson, S., Biessy, B., et al. (2002). A whirling ecosystem in the equatorial Atlantic. *Geophysical Research Letters*, *29*(11), 1553. https://doi.org/10.1029/2001GL014576

Molinari, R. L., Bauer, S., Snowden, D., Johnson, G. C., Bourlès, B., Gouriou, Y., & Mercier, H. (2003). A comparison of kinematic evidence for tropical cells in the Atlantic and Pacific oceans. In G. J. Goni, & P. Malanotte- Rizzoli (Eds.), *IAPSO special issue: Interhemispheric water exchange in the Atlantic Ocean, Elsevier Oceanography Series 68*, (pp. 269–286).

Niiler, P. P., Maximenko, N. A., Panteleev, G. G., Yamagata, T., & Olson, D. B. (2003). Near-surface dynamical structure of the Kuroshio Extension. *Journal of Geophysical Research*, *108*(C6), 3193. https://doi.org/10.1029/2002JC001461

Nobre, P., & Shukla, J. (1996). Variations of sea surface temperature, wind stress, and rainfall over the tropical Atlantic and South America. *Journal of Climate*, *9*(10), 2464–2479. https://doi.org/10.1175/1520-0442(1996)009<2464:VOSSTW>2.0.CO;2

Perez, R. C., Garzoli, S. L., Meinen, C. S., & Matano, R. P. (2011). Geostrophic velocity measurement techniques for the meridional overturning circulation and meridional heat transport in the South Atlantic. *Journal of Atmospheric and Oceanic Technology*, *28*(11), 1504–1521. https://doi.org/10.1175/JTECH-D-11-00058.1

Perez, R. C., Hormann, V., Lumpkin, R., Brandt, P., Johns, W. E., Hernandez, F., et al. (2014). Mean meridional currents in the central and eastern equatorial Atlantic. *Climate Dynamics*, *43*(11), 2943–2962. https://doi.org/10.1007/s00382-013-1968-5

Perez, R. C., Lumpkin, R., Johns, W. E., Foltz, G. R., & Hormann, V. (2012). Interannual variations of Atlantic tropical instability waves. *Journal of Geophysical Research*, *117*, C03011. https://doi.org/10.1029/2011JC007584

Peter, A. C., Le Henaff, M., du Penhoat, Y., Menkes, C. E., Marin, F., Vialard, J., et al. (2006). A model study of the seasonal mixed layer heat budget in the equatorial Atlantic. *Journal of Geophysical Research*, *111*, C06014. https://doi.org/10.1029/2005JC003157

Richter, I., Behera, S. K., Masumoto, Y., Taguchi, B., Sasaki, H., & Yamagata, T. (2013). Multiple causes of interannual sea surface temperature variability in the equatorial Atlantic Ocean. *Nature Geoscience*, *6*(1), 43–47. https://doi.org/10.1038/ngeo1660

Rugg, A., Foltz, G. R., & Perez, R. C. (2016). Role of mixed layer dynamics in tropical North Atlantic interannual sea surface temperature variability. *Journal of Climate*, *29*(22), 8083–8101. https://doi.org/10.1175/JCLI-D-15-0867.1

Sasaki, H., Nonaka, M., Sasai, Y., Uehara, H., & Sakuma, H. (2008). An eddy-resolving hindcast simulation of the quasiglobal ocean from 1950 to 2003 on the Earth simulator. In K. Hamilton, & W. Ohfuchi (Eds.), *High resolution numerical modelling of the atmosphere and ocean*, (pp. 157–185). New York: Springer. https://doi.org/10.1007/978-0-387-49791-4_10

Schmid, C., Molinari, R. L., & Garzoli, S. L. (2001). New observations of the intermediate depth circulation in the tropical Atlantic. *Journal of Marine Research*, *59*(2), 281–312. https://doi.org/10.1357/002224001762882664

van Sebille, E., Baringer, M. O., Johns, W. E., Meinen, C. S., Beal, L. M., de Jong, M. F., & van Aken, H. M. (2011). Propagation pathways of classical Labrador Sea water from its source region to 26°N. *Journal of Geophysical Research*, *116*, C12027. https://doi.org/10.1029/2011JC007171

van Sebille, E., Johns, W. E., & Beal, L. M. (2012). Does the vorticity flux from Agulhas rings control the zonal pathway of NADW across the South Atlantic? *Journal of Geophysical Research*, *117*, C05037. https://doi.org/10.1029/2011JC007684

von Schuckmann, K., Brandt, P., & Eden, C. (2008). Generation of tropical instability waves in the Atlantic Ocean. *Journal of Geophysical Research*, *113*, C08034. https://doi.org/10.1029/2007JC004712

Weingartner, T. J., & Weisberg, R. H. (1991). A description of the annual cycle in sea surface temperature and upper ocean heat in the equatorial Atlantic. *Journal of Physical Oceanography*, *21*(1), 83–96. https://doi.org/10.1175/1520-0485(1991)021<0083:ADOTAC>2.0.CO;2

Weisberg, R. H., J. H. Hickman, T. Y. Yang, and T. J. Weingartner (1987), Velocity and temperature observations during the seasonal response of the equatorial Atlantic experiment at 0°, 28°W.

Weisberg, R. H., Miller, L., Horigan, A., & Knauss, J. A. (1980). Velocity observations in the equatorial thermocline during GATE. In *Oceanography and Surface Layer Meteorology in the B/C Scale*, (pp. 217–248). Pergamon. ISBN: https://doi.org/info:x-wiley/isbn/9781483283661. https://doi.org/10.1016/B978-1-4832-8366-1.50030-3

Weisberg, R. H., & Weingartner, T. J. (1988). Instability waves in the equatorial Atlantic Ocean. *Journal of Physical Oceanography*, *18*(11), 1641–1657. https://doi.org/10.1175/1520-0485(1988)018<1641:IWITEA>2.0.CO;2

Wenegrat, J. O., & McPhaden, M. J. (2015). Dynamics of the surface layer diurnal cycle in the equatorial Atlantic Ocean (0°, 23°W). *Journal of Geophysical Research: Oceans*, *120*, 563–581. https://doi.org/10.1002/2014JC010504

Wu, Q., & Bowman, K. P. (2007). Interannual variations of tropical instability waves observed by the Tropical Rainfall Measuring Mission. *Geophysical Research Letters*, *34*, L09701. https://doi.org/10.1029/2007GL029719

Zebiak, S. E. (1993). Air-sea interaction in the equatorial Atlantic region. *Journal of Climate*, *27*, 1567–1586.

Zhao, J., & Johns, W. E. (2014). Wind driven seasonal cycle of the Atlantic Meridional Overturning Circulation. *Journal of Physical Oceanography*, *44*(6), 1541–1562. https://doi.org/10.1175/JPO-D-13-0144.1